Technical note

A simplified method to account for wall motion in patient-specific blood flow simulations of aortic dissection: Comparison with fluid-structure interaction

Mirko Bonfanti[a,*], Stavroula Balabani[a], Mona Alimohammadi[a], Obiekezie Agu[b], Shervanthi Homer-Vanniasinkam[a,c,d], Vanessa Díaz-Zuccarini[a,*]

[a] Department of Mechanical Engineering, University College London, WC1E 7JE, UK
[b] University College London Hospital, NW1 2BU, UK
[c] Leeds Teaching Hospitals NHS Trust, LS1 3EX, UK
[d] University of Warwick Medical School & University Hospitals Coventry and Warwickshire NHS Trust, CV4 7AL, UK

*** Corresponding authors:**
E-mail addresses: mirko.bonfanti.15@ucl.ac.uk (M. Bonfanti), v.diaz@ucl.ac.uk (V. Díaz-Zuccarini)

https://doi.org/10.1016/j.medengphy.2018.04.014

Abstract

Aortic dissection (AD) is a complex and highly patient-specific vascular condition difficult to treat. Computational fluid dynamics (CFD) can aid the medical management of this pathology, yet its modelling and simulation are challenging. One aspect usually disregarded when modelling AD is the motion of the vessel wall, which has been shown to significantly impact simulation results. Fluid-structure interaction (FSI) methods are difficult to implement and are subject to assumptions regarding the mechanical properties of the vessel wall, which cannot be retrieved non-invasively. This paper presents a simplified 'moving-boundary method' (MBM) to account for the motion of the vessel wall in type-B AD CFD simulations, which can be tuned with non-invasive clinical images (e.g. 2D cine-MRI). The method is firstly validated against the 1D solution of flow through an elastic straight tube; it is then applied to a type-B AD case study and the results are compared to a state-of-the-art, full FSI simulation. Results show that the proposed method can capture the main effects due to the wall motion on the flow field: the average relative difference between flow and pressure waves obtained with the FSI and MBM simulations was less than 1.8% and 1.3%, respectively and the wall shear stress indices were found to have a similar distribution. Moreover, compared to FSI, MBM has the advantage to be less computationally expensive (requiring half of the time of an FSI simulation) and easier to implement, which are important requirements for clinical translation.

Keywords: Computational fluid dynamics (CFD), Fluid-structure interaction (FSI), Aortic dissection, Compliant model, Windkessel model, Blood flow, Moving boundary.

1 Introduction

Aortic Dissection (AD) is a life-threatening vascular condition initiated by a tear in the intima layer that allows the blood to flow within the aortic wall and leads to the formation of two distinct flow channels, the true lumen (TL) and the false lumen (FL), separated by the so-called intimal flap (IF) [1].

The clinical decision-making process around Stanford type-B dissections (i.e. ADs involving only the descending aorta) is complex and patient-specific [2]. Surgical intervention is the preferred choice in the presence of complications, whereas 'uncomplicated' ADs (referring to ADs without complications, such as organ malperfusion, rupture, refractory pain or hypertension, at presentation) [3] are usually managed by controlling the blood pressure [4]. Long-term prognosis of medically treated ADs remains poor, with aortic dilation and late-term complications reported in 25-50% of the cases within 5 years [5].

Patient-specific computational fluid dynamics (CFD) can inform the decision-making process around the disease and aid the identification of patients prone to adverse outcomes by providing detailed information about haemodynamic factors [6–9]. Moreover, numerical models may support clinicians by virtually simulating different interventional strategies [10,11].

The use of three-dimensional (3D) rigid models that neglect the effects that vessel wall motion exerts on the fluid dynamics has been shown to impact simulation results considerably [12]. Vascular compliance, IF motion and the critical role of haemodynamics on AD prognosis (e.g. tear propagation and rupture) necessitate the use of more advanced fluid-structure interaction (FSI) approaches to simulate the flow in this complex aortic condition. FSI couples CFD simulations with finite element modelling (FE) of the aortic wall; however, this method is subject to significant and additional modelling assumptions regarding the mechanical properties of the vessel, which are patient-specific and not known for the case of AD [13]. In addition, FSI models are difficult to setup and demand significant computational effort to be resolved. ADs are arguably one of the most challenging aortic pathologies to simulate and hence it is not surprising that there are only a handful of studies on AD accounting for wall motion in the literature [12,14,15]. Chen et al. [16] recently presented an FSI model of an idealised dissected porcine aorta without re-entry tear, assuming a homogeneous linear-elastic material model. The study presents a first attempt to validate AD FSI simulations against bench experiments.

Two key objectives of patient-specific modelling and simulation for clinical support are a) to gather as much information as possible from the patient, if possible, via non-invasive techniques and b) to perform detailed computations in clinically-meaningful timescales. Neither is currently achievable with FSI due to the lack of patient-specific arterial wall properties and associated high computational costs mentioned above.

However, imaging can help in this respect by providing significant patient-specific detail on the motion of the wall and the IF. With this in mind and in view of the aforementioned limitations of FSI, this paper presents a simplified and computationally efficient method to account for the motion of the IF and vessel compliance in type-B AD CFD simulations, circumventing the need to use full-FSI techniques. The 'moving-boundary method' (MBM) presented here can be tuned with non-invasive patient-specific measurements (e.g. two-dimensional cine magnetic resonance imaging, 2D cine-MRI). It aims at capturing the main fluid dynamic effects due to the fluid-solid interaction by representing the motion of the vessel wall and IF in a simplified, and yet meaningful way. It adopts a physiologically-supported calculation based on pressure differences and fluid forces calculated in the computational domain along with wall stiffness estimated in different regions of the vessel.

A description of the proposed method is presented in the following section, including its validation against the one-dimensional (1D) solution of flow through an elastic straight tube. The MBM is then applied to a type-B AD case, which was previously simulated with full-FSI [12]. In order to directly compare both methods, displacement data available from the FSI simulation was taken as the benchmark upon which the MBM was tuned. Results for both cases are presented and discussed in Section 3, including the comparison of haemodynamic results obtained with the MBM and FSI simulations of the AD case.

2 Methods

2.1 Description of the method

The proposed moving-boundary method (MBM) allows the motion of the 3D model boundaries in a CFD framework by means of a deformable mesh, avoiding the detailed structural analysis of the arterial wall. It is assumed that the vessel wall and IF are in static equilibrium with the fluid forces at each time-step, and that dynamic and viscoelastic effects are negligible. The displacements of the aortic external wall and IF follow the local surface-normal direction, and are linearly related to the fluid forces acting on them. The displacement δ_i [m] of each mesh node *i* on the external vessel wall is prescribed by Eq. 1:

$$\boldsymbol{\delta}_i = \frac{p_i - p_{ext}}{K_i}\ \vec{\mathbf{n}}_i \qquad \text{(Eq. 1)}$$

where p_i [Pa] is the pressure at node *i*, p_{ext} [Pa] is the external pressure set as equal to the diastolic pressure, $\vec{\mathbf{n}}_i$ is the local unit normal vector in the outward direction, and K_i [N/m^3] is a measure of the wall stiffness at node *i*. Under the hypothesis of a circular cross section, K_i can be related to the vessel wall distensibility $\mathcal{D}$ [Pa^{-1}] as follows:

$$K_i = \frac{2}{\mathcal{D}}\sqrt{\frac{\pi}{A_i^0}} \qquad \text{(Eq. 2)}$$

where A_i^0 [m^2] is the diastolic cross-sectional area at the location of node *i*.

The IF is modelled as a zero-thickness membrane and is discretised into a number of patches (i.e. surface regions); the displacement $\boldsymbol{\delta}_j$ [m] of each mesh node on patch *j* is prescribed by Eq. 3:

$$\boldsymbol{\delta}_j = \frac{\overline{\mathbf{F}}_j^{tm}}{K_j\, A_j} \qquad \text{(Eq. 3)}$$

where $\overline{\mathbf{F}}_j^{tm}$ [N] is the surface normal-transmural force (TMF) on patch *j*, considering the viscous and pressure forces acting on both TL and FL sides of the IF patch; A_j [m^2] is the surface area of patch *j*; K_j [N/m^3] is the stiffness coefficient assigned to patch *j*. For each patch, K_j can assume two values, namely K_j^{FL} and K_j^{TL} depending on whether $\overline{\mathbf{F}}_j^{tm}$ points in the direction of the FL or the TL, respectively. Thus, it is possible to account for the different mechanical behaviour that the IF can exhibit in case of extension (i.e. TL expansion) or contraction (i.e. TL compression), as highlighted by Karmonik et al. [17]. The tuning of K_i and K_j is based on patient-specific displacement data obtainable, for instance, from cine 2D MR images.

In this study, the MBM was implemented in ANSYS-CFX 17.0 (ANSYS Inc., PA, USA). The mesh motion was obtained by specifying the displacements of the boundaries following Eqs. 1 and 3, defined in CFX via the CFX Expression Language (CEL) [18]. The mesh displacement equations were solved so as to obtain an implicit two-way coupling between mesh motion and fluid dynamics.

2.2 Flow in an elastic straight tube

The flow through an elastic straight tube was studied to provide a preliminary validation of the proposed method, and to prove its ability to capture wave transmission phenomena. The solution obtained with a 3D model implementing the MBM was compared to the solution of a 1D elastic tube, which is a common approach in the study of wave propagation in the arteries and has been thoroughly validated in the literature [19–21].

The parameters of the tube resemble those of a healthy human aorta, and were taken from Alastruey et al. [20]. The tube has a length l = 40 cm, an initial lumen radius r = 1 cm, a wall thickness h = 1.5 mm and a Young's modulus E = 0.4 MPa. The blood was modelled as a Newtonian fluid (density ρ = 1056 kg/m^3, dynamic viscosity μ = 3.5 cP). At the inlet, a periodic flow waveform was applied, with the systolic phase modelled as a half-sinusoidal waveform, and the diastolic phase as zero-flow [20] (mean flow Q = 3.8 l/min, cycle period T = 0.8 s, systolic phase T_{sys} = T/3). A three-element Windkessel (WK3) model was coupled at the outlet. WK3s are electrical analogues of the downstream vasculature and consist of a proximal resistance, R_1, connected to a compliance, C, and a distal resistance, R_2 (Fig. 1a). WK3 parameters were taken from Alastruey et al. [20] ($R_1 + R_2 = 1.418$ mmHg s ml^{-1}, C = 0.840 ml mmHg^{-1}). R_1 was set equal to the characteristic impedance of the elastic tube (R_1 = 0.155 mmHg s ml^{-1}), and an outflow pressure P_{out} = 9.98 mmHg was considered.

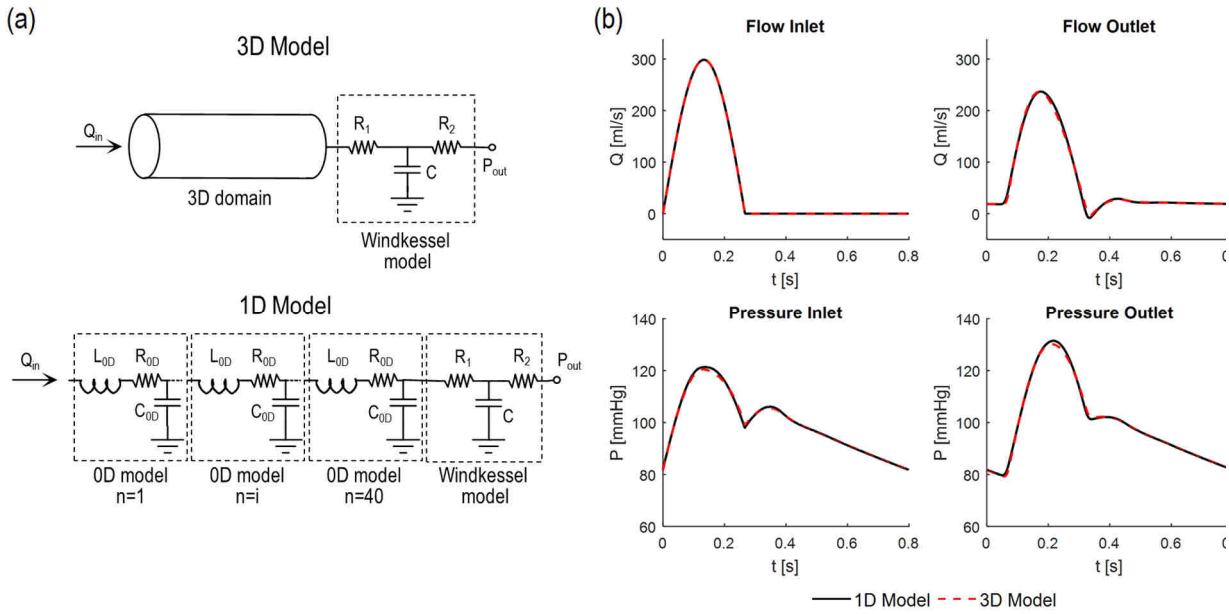

Figure 1: (a) Schematic of the 3D and 1D models of the flow through an elastic tube coupled to a Windkessel model. The 1D model is discretised with N=40 0D LRC models connected in series. (b) Comparison between the flow-rate and pressure waves obtained with the 1D and 3D models at the inlet and outlet of the elastic tube (solid line: 1D model, dashed line: 3D model).

A 3D model of the tube employing the MBM was implemented in ANSYS-CFX 17.0. The parameter K_i was derived from the distensibility of the tube, $\mathcal{D}$, calculated according to Eq. 4 [22]:

$$\mathcal{D} = \frac{3}{2}\frac{r}{Eh}\,. \qquad \text{(Eq. 4)}$$

A 1D model of the elastic tube was implemented in 20-sim (Controllab Products B.V., The Netherlands). As proved by Milišić and Quarteroni [19], a finite number N of lumped parameter (0D) models can discretise a linear continuous 1D model at first-order accuracy in space. Thus, the 1D model was discretised with N = 40 0D models, each of which were made of a resistance R_{0D}, an inductance L_{0D} and a capacitance C_{0D} (Fig. 1a), with parameters calculated according to Rudenick et al. [23]. The resulting equations were solved using the backward Euler method.

The pressure (P) and flow (Q) waves obtained with the 3D and 1D models were compared using the following average relative difference metrics [24]:

$$\Delta\%_{avg,P} = \frac{1}{N_t}\sum_{i=1}^{N_t}\left|\frac{P_i^{3D}-P_i^{1D}}{P_i^{1D}}\right|\,,$$
$$\Delta\%_{avg,Q} = \frac{1}{N_t}\sum_{i=1}^{N_t}\left|\frac{Q_i^{3D}-Q_i^{1D}}{max_j(Q_j^{1D})}\right| \qquad \text{(Eq. 5)}$$

where N_t is the number of time points over a cardiac cycle where the comparison was made (i.e. simulation time-steps in a cardiac cycle). P_i^{1D} and $Q_i^{1D}$are the pressure and flow calculated by the 1D simulation at each time point i at a single location (e.g. tube's inlet or outlet), while P_i^{3D} and $Q_i^{3D}$are the cross-sectional averaged pressure and flow calculated by the 3D simulation at each time point i at a single domain boundary (e.g. tube's inlet or outlet). $\Delta\%_{avg,Q}$ is normalised by the maximum value of flow over the cardiac cycle $max_j(Q_j^{1D})$ to avoid division by small values of flow. The relative difference metrics were calculated once the periodic steady-state was reached in both simulations.

2.3 Aortic dissection case study

The MBM was applied to an AD case study investigated in previous work by Alimohammadi et al. [12] using an FSI methodology; the reader is kindly referred to this publication for details about the FSI model setup.

Table 1: Boundary conditions used for the MBM simulation.

Boundary	Fluid Flow	Mesh Motion
AA – Ascending aorta	Specified inflow waveform [12]	Parallel to boundary surface
BT – Brachiocephalic trunk	Windkessel model	Parallel to boundary surface
LCC – Left common carotid artery	Windkessel model	Parallel to boundary surface
LS – Left subclavian artery	Windkessel model	Parallel to boundary surface
AbAo – Abdominal aorta	Windkessel model	Parallel to boundary surface
External vessel wall	No slip	Specified displacement as per Eq. 1
IF – Intimal flap	No slip	Specified displacement as per Eq. 3

Table 2: Parameters of the Windkessel models used at the outlets of the AD model [12].

	BT	LCC	LS	AbAo
R_1 [mmHg s ml^{-1}]	0.100	0.110	0.150	0.120
R_2 [mmHg s ml^{-1}]	2.480	14.590	11.410	2.118
C [ml mmHg^{-1}]	0.466	0.085	0.110	0.421

2.3.1. Geometry and mesh

The 3D flow domain was generated from the geometry used for the FSI model, representing an acute type-B AD of a 54-year-old female patient. The original geometry was extracted from a computed tomography (CT) scan of the entire aorta performed with a 64-slice Siemens scanner (Siemens AG, Germany; in-plane resolution=0.7 mm, inter-slice distance = 0.7 mm; for details on the image segmentation the reader is referred to our previous work [12]). The geometry did not include the abdominal aortic branches and renal arteries because the CT scan resolution did not allow an accurate segmentation of these small arteries. The surface of the IF was discretised in roughly 200 patches (average surface area = 22 ± 12 mm^2) with the aid of the +NURBS module of ScanIP image-processing software (Synopsys Inc., CA, USA).

The fluid volume was discretised using ICEM-CFD (ANSYS Inc.) with an unstructured tetrahedral mesh in the core region and 7 prism layers at both IF sides and vessel wall, with dimensionless height of the near wall cells (y^+) < 1. The mesh was created using the same parameters adopted for the fine mesh used in the FSI model, for which a mesh sensitivity analysis checking for Time-Averaged Wall Shear Stress (TAWSS), Oscillatory Shear Index (OSI) and velocity variables was carried out, as described in the paper by Alimohammadi et al. [12]. The grid consisted of about 483,000 elements.

2.3.2. Boundary conditions

In order to perform a comparison between the MBM and FSI models, the same CFD boundary conditions (BCs) and fluid properties employed in our previous work [12] were applied to the MBM model. Blood was modelled as an incompressible fluid with a density of 1056 kg/m^3 and a non-Newtonian viscosity described by the Carreau-Yasuda model, with parameters from [25]. The shear-stress transport turbulence model was used with 1% turbulence intensity at the inlet, as in our previous work [12]. The fluid flow and mesh motion BCs are detailed in Table 1. WK3 models were coupled at the outlet branches with parameters shown in Table 2. The mean Reynolds and Womersley numbers, based on the inlet diameter of the aorta, were equal to 831 and 25, respectively. The peak Reynolds number was 4252, which is close to the critical Reynolds number for transition to turbulence calculated as in Peacock et al. [26].

2.3.3. Model-tuning procedure based on displacement data

The clinical dataset available for the studied AD case lacked *in vivo* wall motion images. Thus, as a proof-of-concept of the proposed method and for validation purposes, we used displacement data generated from the FSI simulation [12] to tune the MBM. Nonetheless, the procedure described here can be generalised and implemented using clinically-obtained motion data (e.g. 2D cine-MRI).

The parameter K_i is related to the wall distensibility $\mathcal{D}$ via Eq. 2. $\mathcal{D}$ can be estimated in different aortic regions *k* using Eq. 6 [27]. In this case, we selected the following regions: ascending aorta, upper aortic branches and descending dissected aorta, where different vessel diameter or wall-structure alteration (due to the dissection) would be expected to affect the value of $\mathcal{D}$.

$$\mathcal{D}_k = \frac{\Delta A_k}{A_k^0 \, \Delta p_k} \qquad \text{(Eq. 6)}$$

where ΔA_k [m^2] is the difference between the maximum and minimum area over the cardiac cycle of a vessel cross-section slice in region *k*, in this case determined from FSI wall displacement results; A_k^0 [m^2] is the minimum cross-section area; Δp_k [Pa] is the difference between the maximum and minimum average cross-section pressure estimated from CFD simulations, as described below.

The parameter K_j is tuned to model the IF mechanical response to the TMF. 15 patches out of those into which the IF is discretised were selected along the longitudinal direction of the IF for the tuning. After initial comparison with the FSI results, it was found that the selected number of patches allows to describe the spatial-variability of parameter K_j along the IF, while keeping the amount of information required for the tuning small enough to be obtainable by an MRI protocol. The maximum IF displacements through FL ($\delta_j^{FL,max}$) and TL ($\delta_j^{TL,max}$) over a cardiac cycle are determined from the FSI results at the location of each selected patch. Thus, K_j^{FL} and K_j^{TL} are calculated via Eq. 7:

$$K_j^{FL} = \frac{F_j^{FL,max}}{\delta_j^{FL,max} \, A_j} \; ; \; K_j^{TL} = \frac{F_j^{TL,max}}{\delta_j^{TL,max} \, A_j} \qquad \text{(Eq. 7)}$$

where $F_j^{FL,max}$ and $F_j^{TL,max}$ [N] are obtained from CFD simulations, as explained below, and represent the maximum magnitude of the TMF on patch *j*, when pointing to FL or TL, respectively. The K_j values for the remaining patches are obtained by linearly interpolating the values for the sample patches along the IF axial direction using MATLAB (Mathworks, MA, USA).

The values of Δp_k, $F_j^{FL,max}$ and $F_j^{TL,max}$ were estimated from a rigid-wall CFD simulation. The MBM tuning was refined until the displacement obtained from the MBM was deemed sufficiently close to the FSI results (i.e. less than 0.05 mm of difference for $\delta_j^{FL,max}$ and $\delta_j^{TL,max}$, and less than 0.5% of difference for the cross-sectional area variation $\triangle A_k/A_k^0$).

2.3.4. CFD simulations

The Navier-Stokes equations were solved with ANSYS-CFX 17.0 with a time step of 0.01 s. For each simulation, the periodic steady-state was achieved within 3 cardiac cycles after appropriate initialisation, and the results of the last cycle were used for the analysis.

For comparison purposes, a rigid-wall simulation with the same BCs and geometry of the FSI model was performed. It should be noted that the purpose of running a rigid-wall simulation was not to set-up a 'patient-specific' rigid-wall model, matching the pressures and flow-distribution for the patient under study, but to showcase the effects that wall-deformation alone has on the simulation results. For this reason, the same BCs of the FSI model were used.

3 Results and discussion

3.1 Flow in an elastic straight tube

The solutions obtained with the 3D and 1D models are compared in Fig. 1b. The flow-rate at the tube outlet and pressure waves at the inlet and outlet of the elastic tube are in close agreement ($\Delta\%_{avg,Q}^{outlet} = 0.8\%$, $\Delta\%_{avg,P}^{inlet} = 0.3\%$, $\Delta\%_{avg,P}^{outlet} = 0.4\%$), demonstrating the ability of the MBM approach to model wave propagation due to vessel compliance in a 3D simulation.

3.2 Aortic dissection case study

The pressure and flow-rate waves obtained at the AD model's inlet and outlets with the different methodologies (FSI, MBM, rigid) are shown in Fig. 2.

The MBM and FSI results are in close agreement, with an average relative difference less than 1.8% and 1.3% for the flow and pressure waves, respectively (calculated following Eq. 5, where MBM and FSI were considered instead of 3D and 1D simulations, respectively). A good synchronisation between the

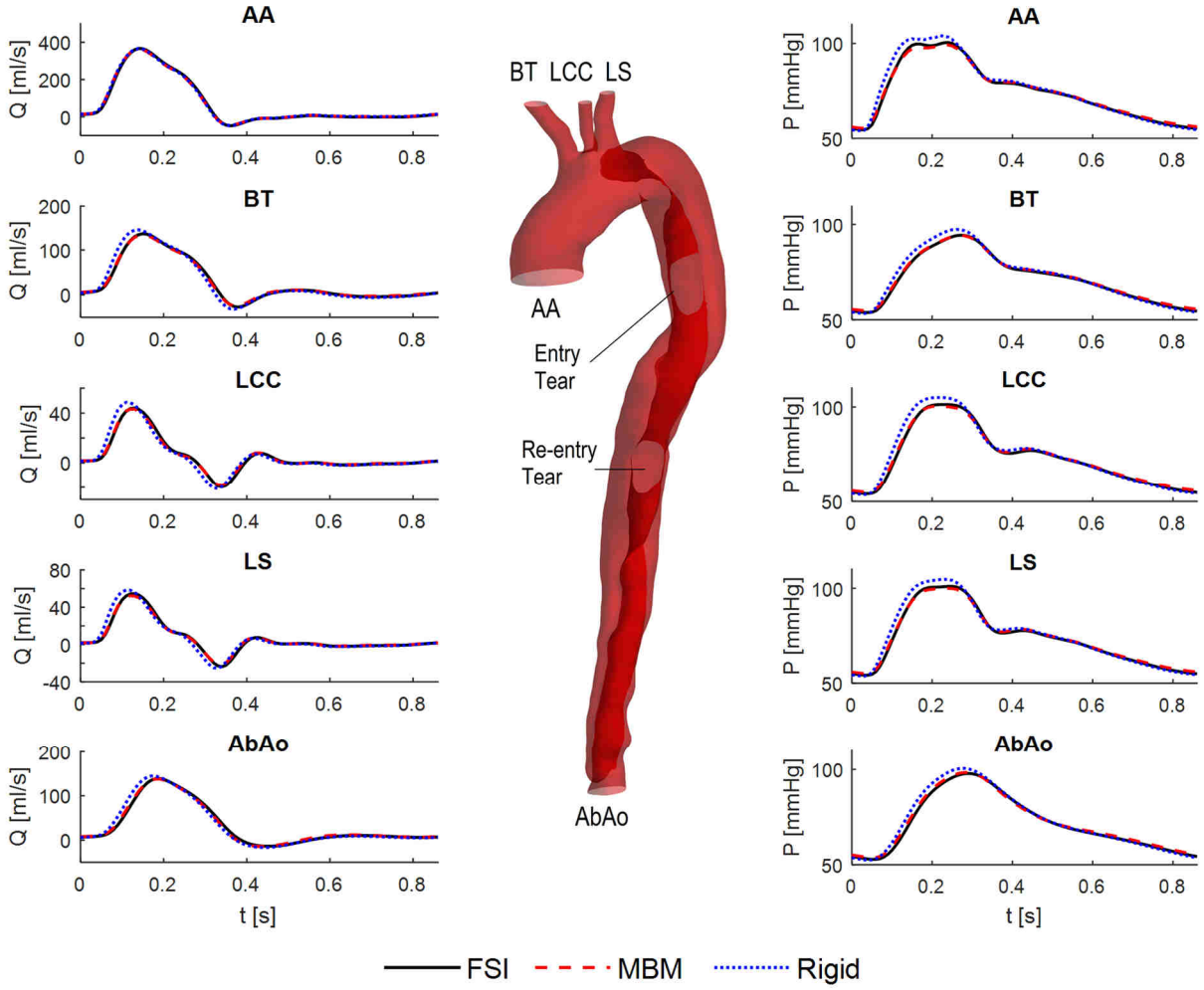

Figure 2: Comparison between pressure and flow-rate waves obtained at the inlet and outlets of the AD model by the FSI (solid line), MBM (dashed line) and Rigid (dotted line) approaches. The reported results refer to the simulations at the periodic steady-state which was determined by comparing the pressure and flow waves obtained in two successive cardiac cycles at the inlet and each outlet. The periodic steady-state was reached when the maximum relative errors between the waves were less than 1%.

waves computed with the two methods can be seen, indicating that the MBM can successfully capture wave transmission phenomena due to vessel compliance.

On the other hand, the flow and pressure waves obtained assuming a rigid wall, as expected, advance noticeably faster and exhibit higher peak values. For instance, the peak pressure predicted at the inlet of the rigid model ($P_{sys,rigid}$ = 104.20 mmHg) is 3.7% higher than that predicted by the FSI simulation ($P_{sys,FSI}$ = 100.52 mmHg), while the MBM simulation reduces the difference to 1.7% ($P_{sys,MBM}$ = 99.15 mmHg).

Wall displacement results at peak-systole (Fig 3a) show that both MBM and FSI models (Fig. 3a) predict similar expansion of the ascending aorta due to the vessel compliance. The same is true for the motion of the IF towards the TL in the distal part of the dissection, where the transmural pressure (TMP) magnitude is higher than the one in the proximal and inter-tear regions (Fig. 3b).

Pressure differences between TL and FL might provide important diagnostic and prognostic information [28], but cannot be easily assessed in the clinic. For instance, higher pressure in the FL can lead to further expansion, or even rupture of the FL, whilst causing a narrowing of the TL [5,7]. The transmural pressure, TMP, obtained with the FSI and MBM

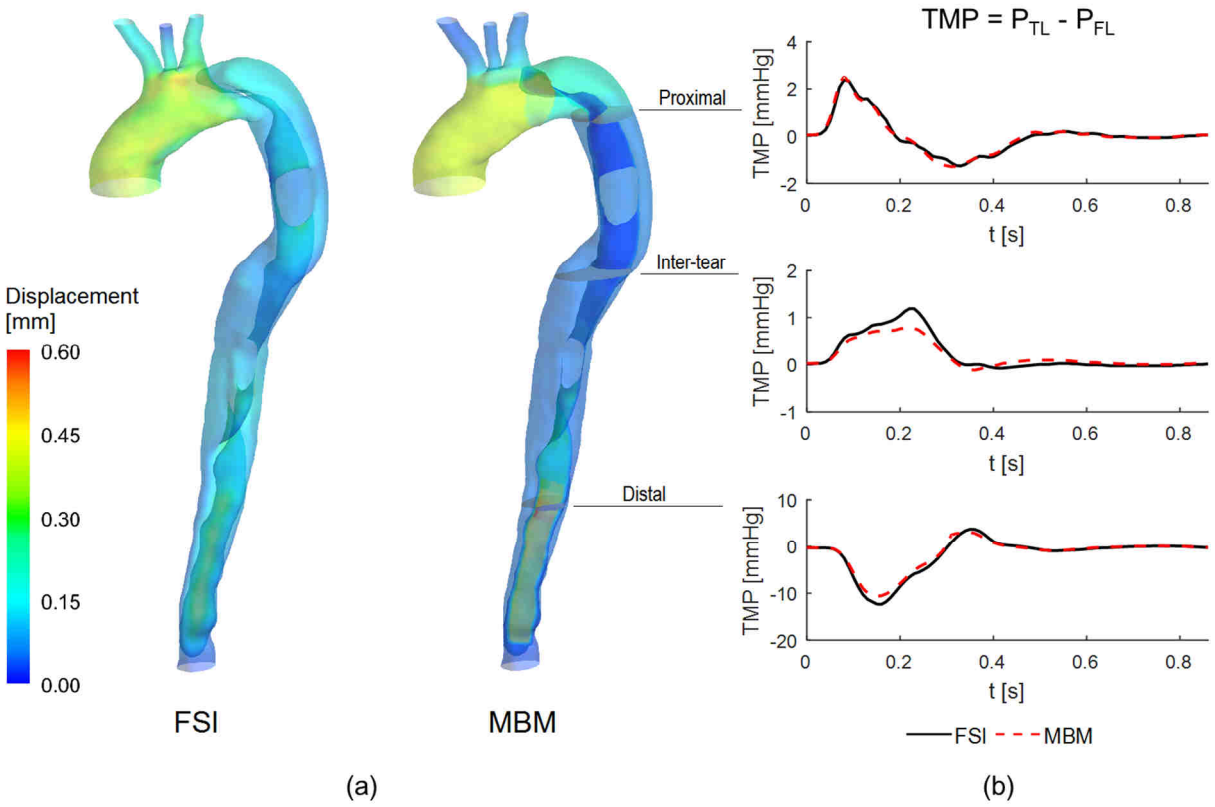

Figure 3: (a) Displacement of the vessel wall and flap at peak systole (t=0.14 s) for the FSI and MBM models. The reported displacement field is relative to the diastolic configuration of the vessel. (b) Comparison between the transmural pressure (TMP) at three different cross-sections obtained with the FSI (solid line) and MBM (dashed line) models.

models at three different locations along the AD is shown in Fig. 3 (TMP = P_{TL} - P_{FL}, where P_{TL} and P_{FL} are the average pressures in the TL and FL, respectively). The TMP curves along the IF are relatively well-matched throughout the cardiac cycle, with a maximum difference of 0.4 mmHg in the inter-tear region of the IF.

Other useful markers that can be extracted from CFD simulations are the Wall Shear Stress (WWS)-based indices, such as the TAWSS and the OSI [29]. WSS is thought to affect the growth and enlargement of the FL [30–32]; for instance, it has been recently reported by Doyle and Norman [5] that areas of low TAWSS may be correlated to regions of rapid local expansion in Type-B AD. The TAWSS distributions obtained with the FSI, MBM and rigid wall models are shown in Fig. 4. The simulations predict qualitatively similar distributions characterised by areas of elevated TAWSS in the upper branches (i.e. BT and LCC) and in the distal TL, and very low TAWSS values in the proximal and distal regions of the FL. The maximum TAWSS value in the distal TL predicted by the MBM method is 23% lower compared to that predicted by the FSI simulation. This difference is attributed to the geometric approximation of the IF as a zero-thickness membrane in the MBM model, which results in a larger TL cross-sectional area (up to +16% in the locations where the TL section is smallest) compared to the FSI model. In contrast, the rigid model overestimates the TAWSS in the TL by around 20% compared to the FSI simulation, as pointed out by Alimohammadi et al. [12]. However, these TAWSS magnitude differences might not be significant in the context of clinical interpretation of the results; most likely any changes to the TAWSS distribution due to, for example, simulated interventions, would be equally well-predicted by all three approaches.

The OSI distributions obtained with the three simulation approaches are reported in Fig. 5. The OSI varies considerably throughout the domain except for the proximal and distal parts of the FL, where the MBM and FSI models predict consistently high values. On the other hand, the rigid model predicts

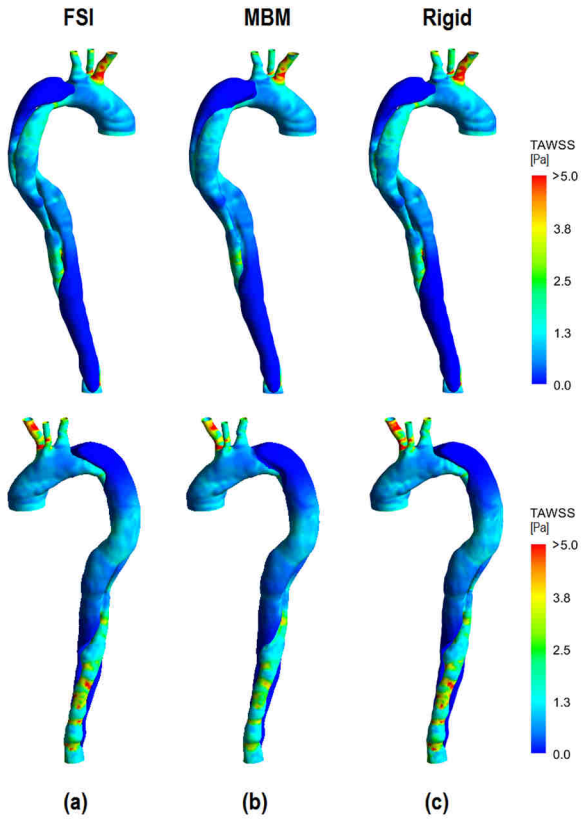

Figure 4: Time-averaged wall shear stress (TAWSS) color maps obtained with the FSI (a), MBM (b), and Rigid (c) models.

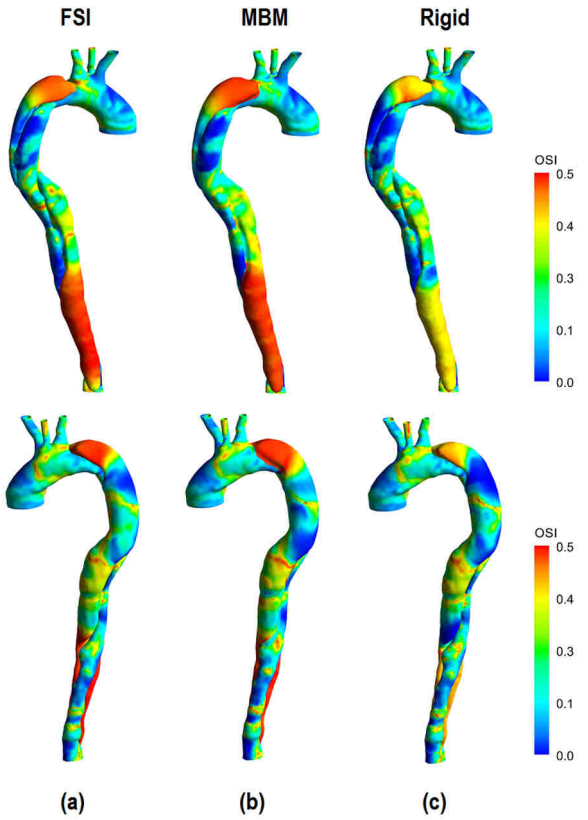

Figure 5: Oscillatory shear index (OSI) color maps obtained with the FSI (a), MBM (b), and Rigid (c) models.

significantly lower OSI in these regions (about -0.15 in absolute values [12]). In fact, the motion of the wall (both in the FSI and MBM models) highly affects the flow in the closed-end parts of the FL, where the alternate expansion and contraction of the vessel due to pressure fluctuations enhances the oscillatory nature of the flow. The correct assessment of WSS-based indices in these regions of the FL can have important prognostic value. For example, as recently reported by Xu et al. [28], the short-term variation of the Relative Residence Time (RRT), which is based on TAWSS and OSI ($RRT = [(1\text{-}2\cdot OSI)\cdot TAWSS]^{-1}$), might be related to the post-TEVAR long-term FL remodelling.

A comparison between the computational requirements of the three simulation approaches is given in Table 3. While the rigid model simulation is significantly faster than the moving-wall ones, the MBM simulation takes only half of the time required by the full FSI simulation. This is because the MBM does not require an FE solver for the description of the vessel structure. The purpose of this method is not to study in detail the deformations and stresses arisen in the vessel tissue, as done by FSI techniques, but to take account of the effects the motion of the vessel induces on the fluid dynamics. These effects usually include a relevant phase-lag of the blood flow and pressure waves between the inlet and outlet of the vessel, a reduction of peak flow-rates and pressures, and a non-zero net flow in the closed-end parts of the vessel lumina that affects clinically relevant WSS-indices, and cannot be captured by rigid-wall simulations.

3.2.1. Limitations

A limitation of the proposed method derives from the approximation of the IF as a zero-thickness membrane. This geometric approximation leads to an error in the lumina's cross-section area, which can affect the computed fluid dynamic variables (e.g. TAWSS) as discussed above. Moreover, the assumption of a circular cross-section used to estimate the vessel distensibility could be critical when the

Table 3: Computational cost of the different approaches.

Method	Mesh: # elements (# nodes)	Simulation time*
FSI	Fluid: 530,077 (184,950) Solid: 145,588 (254,022)	32 h/cycle
MBM	Fluid: 483,126 (217,512)	16 h/cycle
Rigid	Fluid: 459,035 (193,394)	2 h/cycle

* Simulations run on a workstation Intel Xeon E5-2630 v3, 32 GB RAM.

cross-section of the dissected aorta largely deviates from the physiological shape. Due to the high complexity and heterogeneity of ADs, careful consideration needs to be given to each case, and it is up to the modeller to assess if these approximations are appropriate for the specific case under analysis.

The MBM implements a linear, elastic relationship between wall displacement and fluid forces. Although it is well known that the stress-strain relationship of the vessel wall is nonlinear in general, this simplified assumption was considered reasonable for this analysis on the basis of the following grounds: firstly, experimental evidence suggests that the assumption of a linear constitutive relation for the arterial wall is justified in the range of physiological pressures [33]; secondly, the limited availability of data on the viscoelastic properties of the arterial wall in the literature [21] and its alterations in disease, implies that using more advanced constitutive relations would introduce additional complexity and uncertainties on the model parameters.

As discussed in the paper by Alimohammadi et al. [12], the displacements obtained for this case study are comparable to those reported by clinical imaging studies [17,27]. However, in some acute settings, abnormal motion of the IF leading to the obstruction of distal aortic branches can be observed [34]. The upper limit of displacement magnitude that can be resolved by mesh-based computational models is dictated by the deformation of the mesh. Large deformations could lead to poor mesh quality and negative-volume elements, causing the solver to stop. In these cases, the use of automatic re-meshing techniques could be a viable solution [18].

It should be emphasised that in the present study the MBM was tuned using the displacements obtained by an FSI simulation as input, with the purpose of comparing the two methods and validating the proposed approach. However, the MBM can potentially be applied in the clinic using imaging data as input, e.g. cine-MRI, as it has been demonstrated in [15], in which an AD model featuring a compliant wall implemented with the MBM was informed by cine-MRI. Future work will apply the developed tool to study a small cohort of patients for further validation.

4 Conclusions

Through an AD case study, this paper proposes a valid and computationally efficient method (compared to FSI) to account for wall motion in CFD simulations of AD. The good match obtained between MBM and FSI results suggests that the MBM method can capture the relevant effects of the vessel wall motion on the haemodynamics. Compared to FSI, the MBM method has the advantage to be less computationally expensive and easier to implement, which are critical features in the context of clinical use. Moreover, it can be easily tuned with patient-specific vessel motion data obtained non-invasively in the clinic (e.g. via 2D cine MRI) allowing the estimation of the wall stiffness in different regions of the vessel, thus reducing possible errors introduced by using constitutive models with parameters taken from the literature. Since the mesh motion is not imposed, but rather modelled via simple linear equations relating the fluid forces to the displacement of the boundaries, once the parameters have been tuned, the model can be used to simulate different haemodynamic conditions, for instance, allowing the evaluation of possible treatment strategies. In conclusion, this study demonstrates that the MBM is a promising simplified alternative to the more complex and expensive traditional FSI approaches.

Competing interests

The authors declare no conflict of interest.

Funding

This project has received funding from the European Union's Horizon 2020 research and innovation programme under the Marie Sklodowska-Curie grant agreement No 642612, VPH-CaSE (www.vph-case.eu) and from the Leverhulme Trust through the Senior Research Fellowship "Exploring the Unknowable Using Simulation: Structural

Uncertainty in Multiscale Models" (Fellowship number RF-2015-482).

Ethical approval

The study was ethically approved (NHS Health Research Authority, ref: 13/EM/0143). The patient signed the appropriate consent form.

References

[1] Hagan PG, Nienaber C a, Isselbacher EM, Bruckman D, Karavite DJ, Russman PL, et al. The International Registry of Acute Aortic Dissection (IRAD): new insights into an old disease. JAMA 2000;283:897–903. doi:doi:10.1001/jama.283.7.897.

[2] Nienaber CA, Clough RE. Management of acute aortic dissection. Lancet 2015;385:800–11. doi:10.1016/S0140-6736(14)61005-9.

[3] Van Bogerijen GHW, Tolenaar JL, Rampoldi V, Moll FL, Van Herwaarden JA, Jonker FHW, et al. Predictors of aortic growth in uncomplicated type B aortic dissection. J Vasc Surg 2014;59:1134–43. doi:10.1016/j.jvs.2014.01.042.

[4] Goldfinger JZ, Halperin JL, Marin ML, Stewart AS, Eagle KA, Fuster V. Thoracic aortic aneurysm and dissection. J Am Coll Cardiol 2014;64:1725–39. doi:10.1016/j.jacc.2014.08.025.

[5] Doyle BJ, Norman PE. Computational Biomechanics in Thoracic Aortic Dissection: Today's Approaches and Tomorrow's Opportunities. Ann Biomed Eng 2016;44:71–83. doi:10.1007/s10439-015-1366-8.

[6] Dillon-Murphy D, Noorani A, Nordsletten D, Figueroa CA. Multi-modality image-based computational analysis of haemodynamics in aortic dissection. Biomech Model Mechanobiol 2016;15:857–76. doi:10.1007/s10237-015-0729-2.

[7] Cheng Z, Wood NB, Gibbs RGJ, Xu XY. Geometric and Flow Features of Type B Aortic Dissection: Initial Findings and Comparison of Medically Treated and Stented Cases. Ann Biomed Eng 2014;43:177–89. doi:10.1007/s10439-014-1075-8.

[8] Shang EK, Nathan DP, Fairman RM, Bavaria JE, Gorman RC, Gorman JH, et al. Use of computational fluid dynamics studies in predicting aneurysmal degeneration of acute type B aortic dissections. J Vasc Surg 2015;62:279–84. doi:10.1016/j.jvs.2015.02.048.

[9] Karmonik C, Partovi S, Müller-Eschner M, Bismuth J, Davies MG, Shah DJ, et al. Longitudinal computational fluid dynamics study of aneurysmal dilatation in a chronic DeBakey type III aortic dissection. J Vasc Surg 2012;56:260–263.e1. doi:10.1016/j.jvs.2012.02.064.

[10] Alimohammadi M, Bhattacharya-Ghosh B, Seshadhri S, Penrose J, Agu O, Balabani S, et al. Evaluation of the hemodynamic effectiveness of aortic dissection treatments via virtual stenting. Int J Artif Organs 2014;37:753–62. doi:10.5301/ijao.5000310.

[11] Chen D, Müller-Eschner M, Kotelis D, Böckler D, Ventikos Y, Von Tengg-Kobligk H. A longitudinal study of Type-B aortic dissection and endovascular repair scenarios: Computational analyses. Med Eng Phys 2013;35:1321–30. doi:10.1016/j.medengphy.2013.02.006.

[12] Alimohammadi M, Sherwood JM, Karimpour M, Agu O, Balabani S, Díaz-Zuccarini V. Aortic dissection simulation models for clinical support: fluid-structure interaction vs. rigid wall models. Biomed Eng Online 2015;14:34. doi:10.1186/s12938-015-0032-6.

[13] Sommer G, Sherifova S, Oberwalder PJ, Dapunt OE, Ursomanno PA, DeAnda A, et al. Mechanical strength of aneurysmatic and dissected human thoracic aortas at different shear loading modes. J Biomech 2016;49:2374–82. doi:10.1016/j.jbiomech.2016.02.042.

[14] Qiao A, Yin W, Chu B. Numerical simulation of fluid–structure interaction in bypassed DeBakey III aortic dissection. Comput Methods Biomech Biomed Engin 2015;18:1173–80. doi:10.1080/10255842.2014.881806.

[15] Bonfanti M, Balabani S, Greenwood JP, Puppala S, Homer-Vanniasinkam S, Díaz-Zuccarini V. Computational tools for clinical support: a multi-scale compliant model for haemodynamic simulations in an aortic dissection based on multi-modal imaging data. J R Soc Interface 2017;14.

[16] Chen HY, Peelukhana S V., Berwick ZC, Kratzberg J, Krieger JF, Roeder B, et al. Editor's Choice - Fluid-Structure Interaction Simulations of Aortic Dissection with Bench Validation. Eur J Vasc Endovasc Surg 2016;52:589–95. doi:10.1016/j.ejvs.2016.07.006.

[17] Karmonik C, Duran C, Shah DJ, Anaya-Ayala JE, Davies MG, Lumsden AB, et al. Preliminary findings in quantification of changes in septal motion during follow-up of type B aortic dissections. J Vasc Surg 2012;55:1419–1426.e1. doi:10.1016/j.jvs.2011.10.127.

[18] ANSYS Inc. CFX Reference Guide. Release 17. 2016.

[19] Milišic V, Quarteroni A. Analysis of lumped parameter models for blood flow simulations and their relation with 1D models. Mathem Mod Num Anal 2004;38:613–32. doi:10.1051/m2an:2004036.

[20] Alastruey J, Parker KH, Peiro J, Sherwin SJ. Lumped Parameter Outflow Models for 1-D Blood

Flow Simulations: Effect on Pulse Waves and Parameter Estimation. Commun Comput Phys 2008;4:317–36.

[21] Reymond P, Merenda F, Perren F, Ru D. Validation of a One-Dimensional Model of the Systemic Arterial Tree. Am J Physiol - Hear Circ Physiol 2009;297:208–22. doi:10.1152/ajpheart.00037.2009.

[22] Westerhof N, Stergiopulos N, Noble MIM. Snapshots of Hemodynamics. Boston, MA: Springer US; 2010. doi:10.1007/978-1-4419-6363-5.

[23] Rudenick PA, Bijnens BH, Segers P, García-Dorado D, Evangelista A. Assessment of wall elasticity variations on intraluminal haemodynamics in descending aortic dissections using a lumped-parameter model. PLoS One 2015;10:1–17. doi:10.1371/journal.pone.0124011.

[24] Xiao N, Alastruey J, Figueroa CA. A systematic comparison between 1-D and 3-D hemodynamics in compliant arterial models. Int J Numer Method Biomed Eng 2014;30:204–31. doi:10.1002/cnm.2598.

[25] Gijsen FJH, van de Vosse FN, Janssen JD. The influence of the non-Newtonian properties of blood on the flow in large arteries: steady flow in a carotid bifurcation model. J Biomech 1999;32:601–8. doi:10.1016/S0021-9290(99)00015-9.

[26] Peacock J, Jones T, Tock C, Lutz R. The onset of turbulence in physiological pulsatile flow in a straight tube. Exp Fluids 1998;24:1–9. doi:10.1007/s003480050144.

[27] Ganten MK, Weber TF, von Tengg-Kobligk H, Böckler D, Stiller W, Geisbüsch P, et al. Motion characterization of aortic wall and intimal flap by ECG-gated CT in patients with chronic B-dissection. Eur J Radiol 2009;72:146–53. doi:10.1016/j.ejrad.2008.06.024.

[28] Xu H, Li Z, Dong H, Zhang Y, Wei J, Watton PN, et al. Hemodynamic parameters that may predict false-lumen growth in type-B aortic dissection after endovascular repair: A preliminary study on long-term multiple follow-ups. Med Eng Phys 2017;7:35–0. doi:10.1016/j.medengphy.2017.08.011.

[29] Cheng Z, Tan FPP, Riga C V, Bicknell CD, Hamady MS, Gibbs RGJ, et al. Analysis of flow patterns in a patient-specific aortic dissection model. J Biomech Eng 2010;132:51007. doi:10.1115/1.4000964.

[30] Alimohammadi M, Agu O, Balabani S, Díaz-Zuccarini V. Development of a patient-specific simulation tool to analyse aortic dissections: Assessment of mixed patient-specific flow and pressure boundary conditions. Med Eng Phys 2014;36:275–84. doi:10.1016/j.medengphy.2013.11.003.

[31] Gao F, Watanabe M, Matsuzawa T. Stress analysis in a layered aortic arch model under pulsatile blood flow. Biomed Eng Online 2006;5:25. doi:10.1186/1475-925X-5-25.

[32] Wen CY, Yang AS, Tseng LY, Chai JW. Investigation of pulsatile flowfield in healthy thoracic aorta models. Ann Biomed Eng 2010;38:391–402. doi:10.1007/s10439-009-9835-6.

[33] Zhou J, Fung YC. The degree of nonlinearity and anisotropy of blood vessel elasticity. Proc Natl Acad Sci 1997;94:14255–60.

[34] Yang S, Li X, Chao B, Wu L, Cheng Z, Duan Y, et al. Abdominal aortic intimal flap motion characterization in acute aortic dissection: Assessed with retrospective ECG-gated thoracoabdominal aorta dual-source CT angiography. PLoS One 2014;9:1–9. doi:10.1371/journal.pone.0087664.